

# Improving Metal Adsorption on Triethylenetetramine (TETA) Functionalized SBA-15 Mesoporous Silica Using Potentiometry, EPR and ssNMR

Joanna Izabela Lachowicz,\* Abdul-Hamid Emwas, Giulia Rossella Delpiano, Andrea Salis, Marco Piludu, Lukasz Jaremko, and Mariusz Jaremko\*

Nanomaterials have received growing attention in the treatment and diagnosis of neurological disorders because the low blood brain barrier permeability hinders the classical pharmacological approach. Metal ion chelators combined with nanoparticles prove effective in the treatment of neurodegeneration and are under extensive studies. Most chelating agents and metallodrugs compete with endogenous molecules for metal coordination, and do not reach the active site. Determining the competition between metallodrugs and endogenous molecules requires knowing the stability constants of formed metal complexes. In this study, for the first time, potentiometric titrations are used to determine metal complex formation constants, and to quantify ligand content in functionalized materials. This new potentiometric approach allows physico-chemical characterization of mesoporous functionalized materials and their metal adsorption capacity in water solution. The potentiometric results are compared with isotherm models obtained by spectroscopic measurements and yield rewarding data fitting. The potentiometric method described here can be extended to different types of nanostructured materials carrying surface ionizable groups.

(copper  $70 \times 10^{-6}$  M, zinc  $350 \times 10^{-6}$  M, and iron  $340 \times 10^{-6}$  M).<sup>[1,2]</sup> Nanomaterials are receiving high attention in the treatment and diagnosis<sup>[3]</sup> of neurological disorders where the classical pharmacological approach is not effective due to low blood brain barrier (BBB) permeability. An effective drug delivery method is combining of drugs with nanocarriers, for example, polymeric micelles, liposomes, lipid, and polymeric nanoparticles (NPs), that have high BBB affinities.<sup>[4]</sup> Metal ion chelators, which are bound covalently to nanoparticles, can facilitate drug entry into the brain.<sup>[5]</sup>

Desferrioxamine (Desferal) is an iron (Fe), aluminum (Al), copper (Cu), and zinc (Zn) chelator that showed a decrease of AD progression in clinical trials,<sup>[2,6]</sup> even if the low BBB permeability of DFO is still debatable.<sup>[7]</sup> DFO conjugated to polystyrene NPs of 240 nm and examined in

human cortical neurons in vitro prevented A $\beta$  peptide aggregation,<sup>[8]</sup> the main component of the amyloid plaques found in the brains of people with Alzheimer's disease.<sup>[9]</sup> Nevertheless, low bioavailability and high toxicity restrict the use of metal chelators in humans.


Functional nanoparticles are characterized by multiple incorporation of positron emitting radionuclides and signal enhancement in positron emission tomography (PET).<sup>[10]</sup> It has been

## 1. Introduction

Transition metals play pivotal roles in human metabolism in trace amounts but may be toxic when they exceed the tolerance limit. Elevated levels of copper ( $390 \times 10^{-6}$  M), zinc ( $1055 \times 10^{-6}$  M), and iron ( $940 \times 10^{-6}$  M) have been reported for Alzheimer's disease (AD) in brain. This contrasts sharply with metal concentrations found in samples collected from healthy patients

Dr. J. I. Lachowicz  
Department of Medical Sciences and Public Health  
University of Cagliari  
Cittadella Universitaria, Monserrato 09042, Italy  
E-mail: lachowicz@unica.it

Dr. A.-H. Emwas  
Core Labs  
King Abdullah University of Science and Technology (KAUST)  
Thuwal 23955-6900, Saudi Arabia

 The ORCID identification number(s) for the author(s) of this article can be found under <https://doi.org/10.1002/admi.202000544>.

© 2020 The Authors. Published by WILEY-VCH Verlag GmbH & Co. KGaA, Weinheim. This is an open access article under the terms of the Creative Commons Attribution License, which permits use, distribution and reproduction in any medium, provided the original work is properly cited.

G. R. Delpiano, Prof. A. Salis  
Department of Chemical and Geological Sciences  
University of Cagliari  
Cittadella Universitaria, Monserrato 09042, Italy

Dr. M. Piludu  
Department of Biomedical Sciences  
University of Cagliari  
Cittadella Universitaria, Monserrato 09042, Italy

Prof. L. Jaremko, Prof. M. Jaremko  
Division of Biological and Environmental Sciences  
and Engineering (BESE)  
King Abdullah University of Science and Technology (KAUST)  
Thuwal 23955-6900, Saudi Arabia  
E-mail: Mariusz.jaremko@kaust.edu.sa

DOI: 10.1002/admi.202000544

reported that NPs with long-lived isotopes increase signal-to-noise ratio. Among different NPs, mesoporous silica nanoparticles (MSNs) are of high interest as imaging agents,<sup>[3,11]</sup> as well as drug carriers for in vitro and in vivo<sup>[11,12]</sup> experiments. On top of that, MSNs are environment-friendly, and are typically removed from the body through renal clearance.<sup>[13]</sup> Moreover, the particle and pore size, shape, and surface properties of MSNs can be kept under control, making delivery even more feasible for many biomedical applications. Furthermore, the high internal surface area and pore volume of MSNs, work together with the possibility of tuning pore dimensions and mesopore surface chemistry. These properties enable loading of large cargo and tuning the interactions between the cargo and the carrier.

Copper (Cu), gallium (Ga), indium (In), yttrium (Y), and zirconium (Zr) metal ions are commonly used in PET imaging. DFO is a very efficient chelator known for  $^{89}\text{Zr}^{4+}$  ions.<sup>[14]</sup> Recently, pore-expanded MSNs functionalized with DFO were used to complex high quantity of  $^{89}\text{Zr}^{4+}$  and gave a high PET signal in vivo.<sup>[10]</sup>

Most PET contrast metal agents are delivered directly into the bloodstream where they interact with serum proteins. For this reason, the metal complexes do not reach their destination and provoke side effects in imaging. Different proteins and peptides present in the serum can compete with chelating agents for metal ions<sup>[15]</sup> and perturb the species distributions of metal drugs/prodrugs during absorption, distribution, metabolism, and excretion processes. Indeed, it is crucial to know the rate, strength, and nature of binding between metallodrugs and serum proteins in order to better understand the pharmacokinetic properties, transport, as well as the mechanisms of action.

As accurately pointed by Debbie Crans:<sup>[16]</sup> *“The rapidly growing popularity of solid state chemistry and its expansion into the areas of new materials and chemistry of materials has resulted in a grow in achieving the detail and species composition on the atomic level. (...) We can investigate systems at an increasing resolution, however, the processes involved in the studies are becoming less mechanistically focused in their molecular description.”*

Adsorption isotherms are routinely drawn in order to present and determine the binding capacity of a surface,<sup>[17]</sup> but titrations and kinetic consideration are also required to determine the concentration(s).<sup>[17]</sup> Protonation processes<sup>[18]</sup> and simple complex formation reactions have been quantitatively described<sup>[19]</sup> on a surface, but few studies have described surface speciation.

Triethylenetetramine (TETA) dihydrochloride, also commonly known as trientine, is a therapeutic molecule that has been used as a copper-chelating agent for second-line treatment of patients with Wilson's disease for many decades.<sup>[20]</sup> In recent years, it has also been tested as an experimental therapeutic molecule in diabetes, where it improves cardiac structure in patients with diabetic cardiomyopathy and left-ventricular hypertrophy.<sup>[21]</sup> TETA is known for forming stable complexes with copper and zinc ions<sup>[21]</sup> and functionalized SBA-TETA particles could be used as new effective chelators for zinc and copper ions in human organs.

In this study, several biophysical methods such as potentiometry, electron paramagnetic resonance (EPR), UV-vis, and solid-state nuclear magnetic resonance (ssNMR) spectroscopy were extensively and successfully used for characterization of SBA-TETA particles. Moreover, potentiometric titrations were used, to the best of our knowledge, for the first time to quantify ligand content in a functionalized nanostructured material and

to determine metal complex formation constants. We present this new potentiometric approach for the physico-chemical characterization of mesoporous functionalized materials and their metal adsorption capacity in water solution.

## 2. Experimental Section

### 2.1. Chemicals

Pluronic copolymer P123 (EO20PO70EO20) tetraethylorthosilicate, TEOS ( $\geq 99\%$ ); (3-chloropropyl)trimethoxysilane, CPTMS ( $\geq 97\%$ ); triethylenetetramine, TETA ( $\geq 97\%$ ); copper chloride dihydrate,  $\text{CuCl}_2 \cdot 2\text{H}_2\text{O}$  ( $\geq 99.0\%$ ),  $\text{ZnCl}_2$  ( $\geq 99.0\%$ ) anhydrous toluene ( $\geq 99.7\%$ ), dimethylformamide (DMF,  $\geq 99.9\%$ ), acetone ( $\geq 99\%$ ), HCl (37%), NaCl, NaOH pellets were purchased from Sigma-Aldrich (Milano, Italy). Copper ( $1000 \pm 2$  ppm in  $\text{HNO}_3$  2% m/m) and zinc ( $1000 \pm 2$  ppm in  $\text{HNO}_3$  1% m/m) stock solutions were purchased from Fluka Analytical and Aldrich Chemical Company, respectively. Diethyl ether (99.8%), and ethanol (99.8%) were purchased from Honeywell.

### 2.2. Synthesis of Mesoporous Materials

SBA-15 mesoporous silica was synthesized and functionalized with CPTMS according to the method described in the previous work.<sup>[21]</sup> Briefly, the functionalization with chloro-propyl group was carried out by dispersing 1 g of obtained SBA-15 in 25 mL of anhydrous toluene, adding 700  $\mu\text{L}$  of CPTMS<sup>[21]</sup> and keeping the mixture under stirring at 110 °C overnight. The resulting SBA-Cl was collected by filtration, washed with  $\text{Et}_2\text{O}$  and water, and dried under vacuum.

0.5 g of SBA-Cl were dispersed in 14 mL of anhydrous toluene, then the green solution of the ligand (0.56 g of TETA dissolved in 1 mL of DMF) was added and the resulting mixture was kept under stirring at 110 °C for 24 h. The dark-yellowish suspension of SBA-TETA was recovered by filtration, washed with  $\text{H}_2\text{O}$ ,  $\text{EtOH}$ , and  $\text{Et}_2\text{O}$ , and dried under vacuum overnight.

SBA-NH<sub>2</sub> was synthesized as a reference material for UV-vis metal coordination studies. The procedure and characterization are described in the previous paper.<sup>[22]</sup>

### 2.3. Physico-Chemical Characterizations

TEM imaging was performed using a Titan CT (Thermo Fisher Scientific) operating at 300 kV equipped with a  $4 \text{ k} \times 4 \text{ k}$  CCD camera (Gatan, Pleasanton, CA, USA). Images were acquired in bright field using a 100  $\mu\text{m}$  objective aperture under parallel illumination.

$\text{N}_2$  adsorption/desorption isotherms at 77 K were carried out on an ASAP 2020 instrument to obtain textural parameters of the materials such as the surface area (Brunauer-Emmett-Teller, B.E.T. theory), pore width, and distribution (Barrett-Joyner-Halenda, B.J.H. theory).<sup>[23]</sup> Before analysis, SBA-15 samples were heated at 110 °C at a rate of  $1^\circ\text{C min}^{-1}$  under vacuum for 12 h, whereas functionalized samples were outgassed under the same conditions while heating at 80 °C.

FT-IR analysis, to verify the presence of chloro-propyl group and TETA, was carried out with a Bruker Tensor 27 spectrophotometer equipped with a diamond-ATR accessory and a DTGS detector. A number of 128 scans at a resolution of  $2\text{ cm}^{-1}$  were averaged in the spectral range  $4000\text{--}400\text{ cm}^{-1}$ . To quantify the functionalization percentage, Elemental Analysis (PerkinElmer Series II 2400) and Thermogravimetric Analysis—TGA (Perkin-Elmer) were performed.

## 2.4. Potentiometric Measurements

Potentiometric titrations were performed in  $0.1\text{ M NaCl}$  at  $298.1 \pm 0.1\text{ K}$  using an automated Mettler Toledo titrator. The thermostated glass-cell was equipped with a magnetic stirrer system, a Mettler Toledo glass electrode, a microburet delivery tube, and an inlet–outlet tube for Argon. The combined Mettler Toledo electrode was calibrated as a hydrogen-ion concentration probe by titrating previously standardized amounts of HCl with  $\text{CO}_2$ -free NaOH solutions and determining the equivalence point by Gran's method,<sup>[24]</sup> which gave the standard potential,  $E^\circ$ , and the ionic product of water ( $\text{pK}_w = 13.74(1)$  in  $0.1\text{ M NaCl}$  at  $298.1\text{ K}$ ). The computer program HYPERQUAD2013<sup>[25]</sup> was used to calculate ligand (TETA or -OH) content (in mmol) in MMs material, MMs-ligand protonation, and complex stability constants from potentiometric data. The potentiometric titrations were prepared from acidic to alkaline conditions (the studied pH range  $2.5\text{--}11.0$ ). Solutions at  $0.1\text{ M}$  ionic strength in NaCl were titrated at  $25.0\text{ }^\circ\text{C}$  with  $0.1\text{ M NaOH}$ . The activity of the species present in the solution was proportional to concentration, where the proportionality constant was the activity coefficient that brings the stoichiometric constant close to the thermodynamic constant. For this reason, the ionic strength was kept constant during experimental determinations of stability constants. Carbonate free sodium hydroxide solutions were prepared according to Albert and Serjeant.<sup>[26]</sup> An mV signal drift module was used to reach equilibrium after each base addition and obtain optimal accuracy of measurements. The metal concentration in  $\text{ZnCl}_2$  and  $\text{CuCl}_2$  stock solutions in HCl was determined by EDTA titration. The MMs were stored at  $50\text{ }^\circ\text{C}$  and cooled in a desiccator to room temperature before being weighed (analytical weight scale, precision  $\pm 0.01\text{ mg}$ ). The working MMs content was  $2.5\text{--}2.7\text{ mg}$  in  $20\text{ mL}$  of water. The total mmol of the ligand in the functionalized MMs was determined by the NaOH titration and metal complex formation studies were performed at 2:1, 1:1, and 1:2 metal/ligand molar ratios. Each measurement, both for ligand protonation and metal-complex experiments, was repeated at least two times in order to verify the repeatability. The different titration curves were calculated as separated curves without significant variations in the values of the calculated stability constants. Finally, the sets of data were merged and treated simultaneously to give the final stability constants. Different equilibrium models for the complex systems were generated by eliminating and introducing different species. Only those models for which the HYPERQUAD program furnished a variance of the residuals  $\sigma^2 \leq 9$  were considered acceptable. Such a condition was unambiguously met by a single model for each system.

The equilibrium concentrations of various species were computed by solving the system of mass balance equations

constructed for each component (Equations (1)–(3) for a system containing three components: M, L, and H), and these mass balance equations were then solved iteratively for the concentrations of the free components.<sup>[27]</sup> In addition, it was necessary to know the stoichiometry and overall/cumulative stability constants ( $\beta(\text{M}_p\text{L}_q\text{H}_r)$ ) of all associations (e.g., ligand species,  $\text{LH}_r$ ; metal complexes,  $\text{M}_p\text{L}_q\text{H}_r$ ; and metal hydrolysis products,  $\text{M}_p\text{H}_r$ ; where  $p$ ,  $q$ , and  $r$  are the stoichiometric numbers of the components in the given species) and the ionization constant of water ( $\text{K}_w$ ).  $\beta(\text{M}_p\text{L}_q\text{H}_r)$  was defined for the general equilibrium shown in Equation (4), where M denotes the metal ion and L is the completely deprotonated ligand

$$C_M = [\text{M}] + \sum_{i=1}^n p_i \beta_{pqr} [\text{M}]^{p_i} [\text{L}]^{q_i} [\text{H}]^{r_i} \quad (1)$$

$$C_L = [\text{L}] + \sum_{i=1}^n p_i \beta_{pqr} [\text{M}]^{p_i} [\text{L}]^{q_i} [\text{H}]^{r_i} \quad (2)$$

$$C_H = [\text{H}] + \sum_{i=1}^n p_i \beta_{pqr} [\text{M}]^{p_i} [\text{L}]^{q_i} [\text{H}]^{r_i} \quad (3)$$

$$p\text{M} + q\text{L} + r\text{H} \leftrightarrow \text{M}_p\text{L}_q\text{H}_r, \text{ as } \beta(\text{M}_p\text{L}_q\text{H}_r) = [\text{M}_p\text{L}_q\text{H}_r] / [\text{M}]^p [\text{L}]^q [\text{H}]^r \quad (4)$$

### 2.4.1. HySS Software Theoretical Calculations

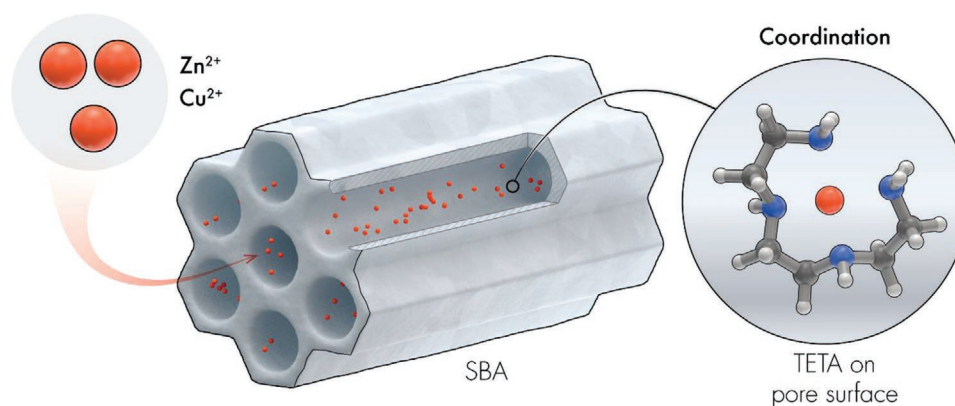
Various computer programs were developed to produce distribution diagrams for the species formed in solution, such as HySS.<sup>[25]</sup> Species distribution curves represented the percentages (or partial mole fractions) or equilibrium concentrations of the different chemical species present in a solution under given conditions in a representative manner.<sup>[28]</sup> Concentration distribution curves were generally presented as a function of a single variable, such as pH, where the fixed values of the components (reagents) uniquely determined the molar ratios of the species formed.

The speciation distribution curves calculated for compounds containing dissociable protons represented the fractional contribution of each protonated ( $\text{LH}_r$ ) and unprotonated (L) species in equilibrium, and thus the average number of protons bound and the actual charge of the ligand could be viewed as a function of the pH.

In these studies, HySS software<sup>[25]</sup> was used to calculate speciation plots of free ligand (Scheme 1, Figure 1), metal complexes (Figure 2), and copper and zinc hydrolysis (Figure S3, Supporting Information) as a function of pH. The curves were calculated on the basis of proper constants: ligand protonation constants, ligand protonation constants and its metal complex formation constants, and metal hydrolysis constants, respectively. The ligand and metal concentrations used for the calculations were the same as experimental data.

The theoretical competition studies were calculated on the base of SBA-TETA protonation constants (Table 1) and complex formation constants (Table 2). The speciation diagrams (Figure 4) were calculated with the ligand and metal concentrations used in experimental competition studies with inductively coupled plasma optical emission spectrometry (ICP-OES) analysis. Moreover, the free metal concentration was calculated at pH 4.





**Scheme 1.** Schematic representation of SBA-TETA material and metal coordination process by TETA ligand. [Images produced by KAUST scientific illustrators. This image is original and designed specifically for the targeted publication. It should not be cropped, distorted, or in any way edited without the expressed consent of Research Publication Services. Because KAUST owns the copyright of the original image, you may cause a copyright conflict between the journal and KAUST if you modify the illustration in any way before submitting it to the journal. Any other use of the image apart from your paper (e.g., in a presentation, poster, or website) should be accompanied by credits to the journal in which it is published and to the illustrator as follows: Xabier Pita/KAUST].

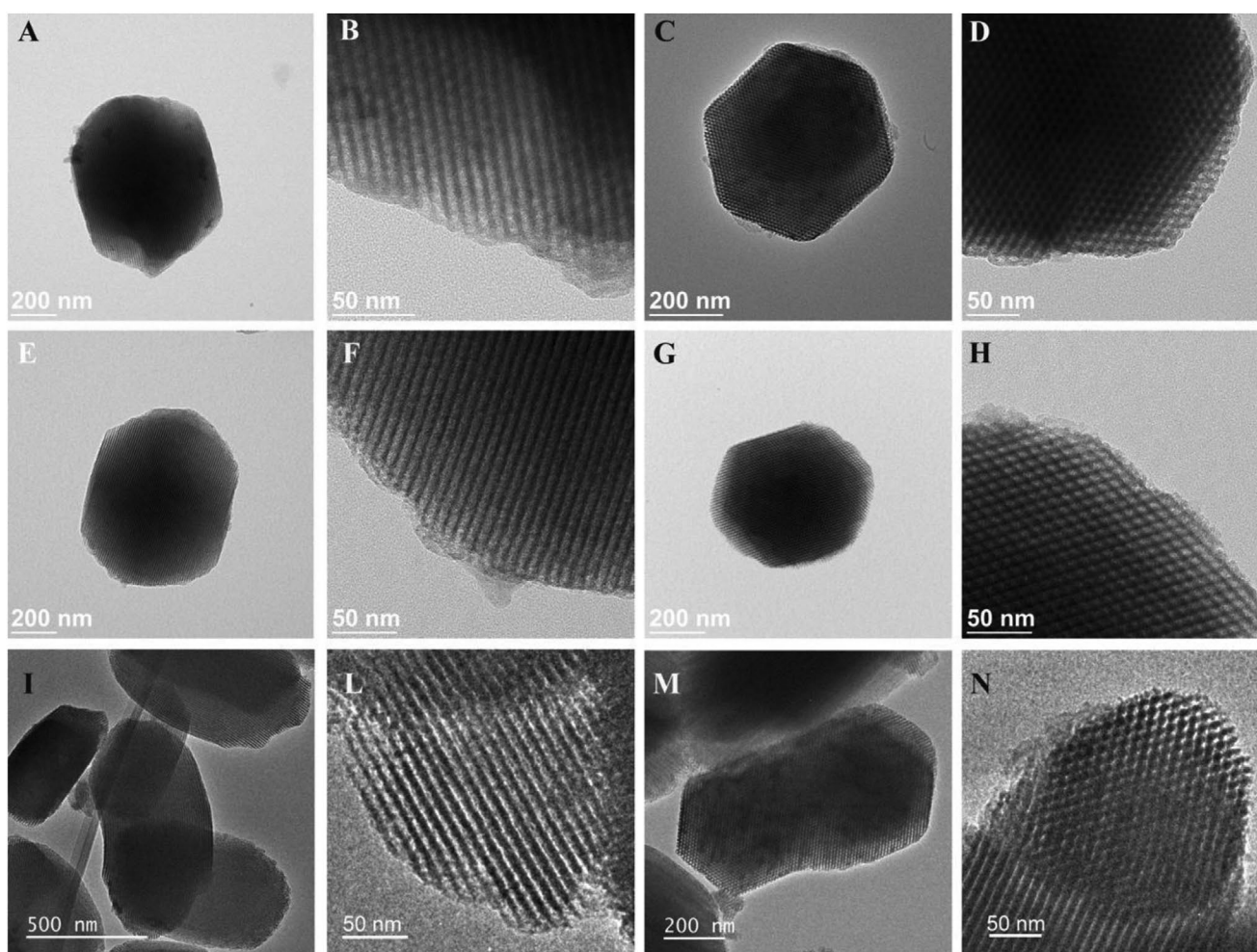


**Figure 1.** A–D) Transmission electron micrographs of SBA-TETA, E–H) SBA-TETA with copper ions, and I–N) SBA-TETA with zinc ions. TEM analysis highlights a well-structured mesoporous structure in all samples. Comparing their side views (A,B,E,F,I,L) and their top views (C,D,G,H,M,N) no evident structural differences are observed.

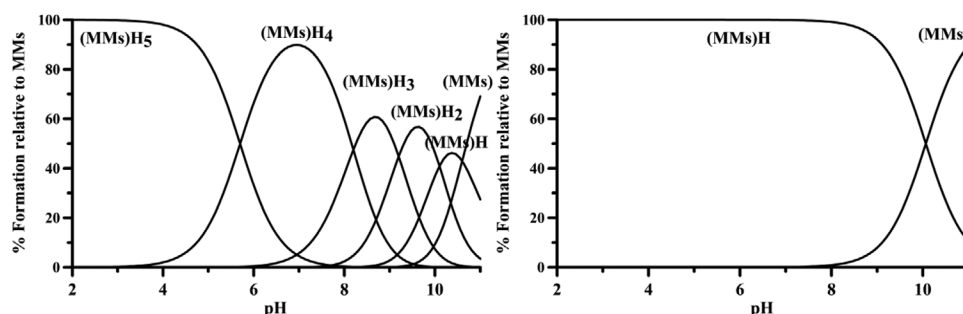


**Figure 2.** Speciation plots relative to the protonation of SBA-TETA (left) and SBA-15 (right). Charges are omitted for simplicity.

The HySS program was also used to calculate the  $pM(\text{etal})$  value for each studied ligand. The negative logarithm of the concentration of the free metal in solution, was calculated for total [ligand] =  $10^{-5}$  M and total [metal] =  $10^{-6}$  M in solution at proper pH (Table 3). For the sake of comparison with literature data, the pH of 7.4 was chosen for the pCu and pZn calculations. Moreover, pCu e pZn values for SBA-TETA in different pHs were calculated (Figure 3).

## 2.5. ICP-OES Competition Studies

The copper and zinc concentrations in aqueous solutions were analyzed by ICP-OES (Agilent 5100). The operational parameters were: RF power: 1.2 kW. Plasma gas:  $12 \text{ L min}^{-1}$ , Aux gas:  $1.0 \text{ L min}^{-1}$ , and nebulizer flow  $0.7 \text{ L min}^{-1}$ . Emission lines (nm): Cu (327.395, 324.754, and 213.598) and Zn (213.857, 202.548, and 206.200). No spectral interference was observed. The standard solutions: 0.5–50 ppm in 1% nitric acid were prepared by the analytical dilution of standard zinc and copper solutions for linear calibration curve ( $R^2 = 0.999$ ).

A mass of 15 mg of SBA-TETA were incubated for 24 h in 25 °C with the copper and zinc 10 ppm solution and in the solution containing 10 ppm copper and 100 ppm zinc ions at pH 4. The process was stopped by filtration of the suspension, then the metal concentration in the solution was quantified through ICP-AES measurements.

## 2.6. Spectroscopies

SBA-15, SBA-NH<sub>2</sub>, and SBA-TETA (20 mg each) were dissolved in 0.123 M copper solution in water (pH = 2.8). After 24 h rotation at room temperature, the solutions were centrifuged and

lyophilized (Figure S4A, Supporting Information). In the next step, the samples were re-hydrated, centrifuged, and dried in the vacuum (Figure S4B, Supporting Information). Successively, the solid-state samples were analyzed by UV-vis.

SBA-TETA, (100 mg) were dissolved in 2 mL of ZnCl<sub>2</sub> and CuCl<sub>2</sub> solutions (0.88 M, pH 4, filtered  $0.2 \times 10^{-6}$  M) and rotated (15 rpm) for 24 h. Afterward, the solutions were centrifuged (14 000 rpm, 30 min) and dried under vacuum. The samples were studied by ssNMR and EPR, respectively.

### 2.6.1. Nuclear Magnetic Resonance

All NMR experiments were performed on Bruker 400 MHz AVANACIII NMR spectrometer at magnetic field strength of 9.4 T with resonating <sup>13</sup>C corresponding frequency of 100.04 MHz. The spectrometer was equipped with 4 mm Bruker double resonance MAS probe (BrukerBioSpin, Rheinstetten, Germany). All <sup>13</sup>C NMR spectra were recorded under the same conditions and parameters with 14 and 12 kHz spinning rate using cross polarization CP pulse program.

The <sup>13</sup>C signals were referenced to the methylene signal of adamantane at 37.78 ppm. Bruker Topspin 3.5pl7 software (Bruker BioSpin, Rheinstetten, Germany) was used for data collection and for data analysis.

### 2.6.2. EPR Spectroscopy

Bruker EMX PLUS spectrometer equipped with standard resonator for high sensitivity CW-EPR (Bruker BioSpin, Rheinstetten, Germany) was used to record all EPR spectra. The operating frequency was set (9.384688 GHz) and the microwave power was set to 0.625 mW with 5 G modulation

**Table 1.** Protonation constants (log K) of SBA-TETA and SBA-15 at 25.0 °C and 0.1 M NaCl, in comparison with log K literature data<sup>[20]</sup> of free TETA. L refers to ligand; free TETA, TETA grafted on MMs material, -OH on SBA-15 material, respectively.

Specie	TETA		Specie	SBA-TETA		SBA-15	
	log β	log K		log β	log K	log β	log K
(L)H	9.79(5)	9.79	(L)H	10.6(2)	10.6	10.0(1)	10.0
(L)H <sub>2</sub>	18.90(4)	9.11	[(L)H <sub>2</sub> ] <sup>+</sup>	20.7(1)	10.1		
(L)H <sub>3</sub>	25.58(2)	6.68	[(L)H <sub>3</sub> ] <sup>2+</sup>	29.9(1)	9.2		
(L)H <sub>4</sub>	28.86(2)	3.28	[(L)H <sub>4</sub> ] <sup>3+</sup>	38.1(1)	8.2		
			[(L)H <sub>5</sub> ] <sup>4+</sup>	43.8(2)	5.7		

**Table 2.** Complex formation constants of TETA,<sup>[20]</sup> SBA-TETA, and SBA-15 with Cu<sup>2+</sup> and Zn<sup>2+</sup> at 25 °C, 0.1 M NaCl ionic strength, obtained from potentiometric data using the Hyperquad program. \*Negative logarithm of the concentration of the free metal in solution, calculated for total [ligand] = 10<sup>-5</sup> M and total [metal] = 10<sup>-6</sup> M at pH 7.4. L refers to ligand: free TETA, TETA grafted on MMs material, -OH on SBA-15 material, respectively.

Specie	TETA				SBA-TETA				SBA-15				
	Cu		Zn		Cu		Zn		Cu		Zn		
	log β	log K	log β	log K	log β	log K	log β	log K	log β	log K	log β	log K	
[MLH <sub>4</sub> ] <sup>5+</sup>					46.08(8)		44.0(3)						
[MLH <sub>3</sub> ] <sup>4+</sup>					42.0(1)	4.08	38.97(4)	5.03					
[MLH <sub>2</sub> ] <sup>3+</sup>					37.19(8)	4.84	32.48(5)	6.49					
[MLH] <sup>2+</sup>	23.4(1)		18.06(6)		30.8(1)	6.39	25.54(5)	6.94			-1.7(1)		
[ML] <sup>+</sup>	20.3(1)	3.1	12.24(3)	5.82	23.4(1)	7.4	17.77(5)	7.77	-5.80(7)				
[MLH <sub>1</sub> ]			2.90(6)	9.34									
pM*		17.1		8.4		16.1		10.8		7.5			6.0

amplitude and 100 kHz modulation frequency. Bruker Xenon software (Bruker BioSpin, Rheinstetten, Germany) was used to collect data and for post processing.

### 2.6.3. UV-Vis Spectroscopy

UV-vis spectra were recorded on Agilent CARY 60 spectrophotometer equipped with a photomultiplier tube detector. Spectra were collected in the wavelength range 200–900 nm with a band width of 5.0 nm and at rate of 200 nm min<sup>-1</sup>.

## 3. Results and Discussion

### 3.1. Physico-Chemical Characterizations

SBA-15 mesoporous silica was synthesized and then functionalized CPTMS and with TETA to obtain SBA-Cl and SBA-TETA (Scheme 1), respectively. The physico-chemical characterizations (SAXS, TEM, FTIR, N<sub>2</sub> adsorption isotherms, TGA) of the obtained samples<sup>[21]</sup> are reported in Figure S1 and Table S1, Supporting Information.

Analysis of all SBA-TETA samples by TEM in bright field mode revealed the typical mesoporous structure that resulted mainly characterized by the presence of ordered pore channels (Figure 1). In side view (Figure 1A,B,E,F,I,L) they appeared as parallel channels in bright contrast, whereas the top views of the same samples (Figure 1C,D,G,H,M,N) highlighted the ordered hexagonal array of the pores. The above results point out that all examined samples (before and after Cu<sup>2+</sup> and Zn<sup>2+</sup> ions loading)

**Table 3.** The comparison of theoretical (HySS) and experimental (ICP-AES) results of copper and zinc competition studies.

Metal ion	Experiment 1		Experiment 2		
	Cu [ppm]	Zn [ppm]	Cu [ppm]	Zn [ppm]	
Initial	10.00	10.00	10.00	100.00	
Final <sup>a)</sup>	HySS	0.10	0.20	0.08	64.97
	ICP-OES	0.01	1.20	3.20	81.70

<sup>a)</sup>After 24 h incubation at pH 4 and 25 °C.

share similar structure, being characterized by analogue hexagonal pore array and uniform pore size and no differences concerning their mesoporous structure were observed.

## 4. Protonation and Metal Complex Equilibria

The stability constants determined in potentiometric titrations can be used in calculating distributions and concentrations of metal species even in complex systems containing many ligands and metal ions, such as biological fluids (e.g., blood serum or gastric juice) and environmental solutions (e.g., sea water or natural water).<sup>[29]</sup> Detailed discussions of chemical speciation in various biological fluids and tissues as well as examples of the application of various methods for determining the distribution of trace elements in biological systems are provided.<sup>[30]</sup>

The aims of our potentiometric studies are as follows: i) obtaining full descriptions of equilibria, including the distribution of the species in the equilibrium system and determining their characteristics, such as solution structures (binding modes) of the species that are in equilibrium with each other; and ii) using equilibrium descriptions of these systems in modeling calculations to determine the species distributions of the constituents in conditions where experimental measurements cannot obtain data, for example, due to extremely low analytical/total concentrations.

SBA-TETA and SBA-15 were characterized through potentiometric titrations. As shown in Scheme 1, TETA molecule has four amino groups and hence four protonation constants (Table 1). The first two constants, log K<sub>1</sub> and log K<sub>2</sub>, are related to the protons bound to the two-terminal primary-amine groups (-NH<sub>2</sub>), while log K<sub>3</sub> and log K<sub>4</sub> constants are related to the protonation of the two secondary amine groups (NH). Potentiometric measurements of SBA-15 (Table 1) showed the presence of one protonation constant at pH 10.0 due to the dissociation of silanols (SiOH) into SiO<sup>-</sup>. A more acidic constant, not observed in our experiment, due to the protonation of SiOH into SiOH<sub>2</sub><sup>+</sup>, should occur at pH < 2.<sup>[31]</sup>

SBA-TETA has five protonation constants, which can be attributed to the four nitrogen atoms of TETA and to free Si-OH, which may still occur also after SBA-15 functionalization. Indeed, the occurrence of free silanol groups in SBA-TETA

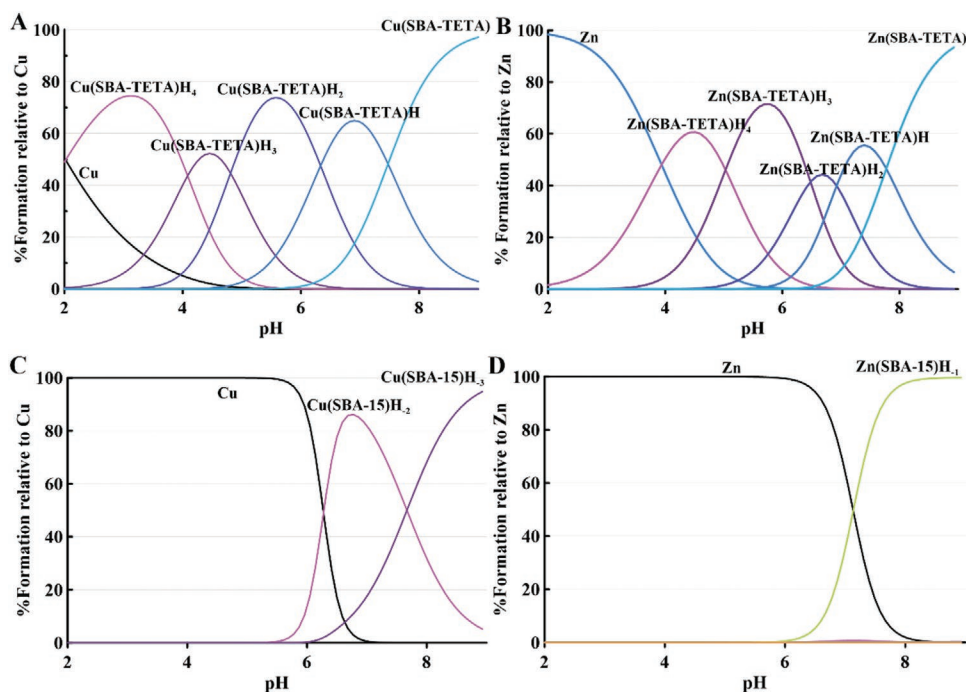


**Figure 3.** Speciation plots of A,B) SBA-TETA ( $[TETA] = 1.00 \times 10^{-4}$  M,  $[Cu^{2+}] = 1.00 \times 10^{-4}$  M, and  $[Zn^{2+}] = 5 \times 10^{-5}$  M) and C,D) SBA-15 ( $[-OH] = 1.00 \times 10^{-3}$  M,  $[Cu^{2+}] = 1.00 \times 10^{-4}$  M, and  $[Zn^{2+}] = 1 \times 10^{-4}$  M) metal complexes calculated on the basis of stability constants reported in Table 3. Charges are omitted for simplicity.

was confirmed by the FTIR band at  $960\text{ cm}^{-1}$  (Figure S2B, Supporting Information). Hence, the highest protonation constants of SBA-TETA could be assigned to Si–OH dissociation ( $\log K = 10.6$ ) and the terminal nitrogen atoms of grafted TETA ( $\log K = 10.1; 9.2$ ), respectively (Table 1). Analogously to free TETA, the remaining two protonation constants ( $\log K = 8.2; 5.7$ ) are assigned to the inner nitrogen atoms. By comparing  $\log K$  values for free TETA and SBA-TETA a general shift toward higher pH is observed. This shift could be due to the presence of intramolecular hydrogen bonds, which makes proton dissociation more difficult for SBA-TETA compared to the free ligand.<sup>[32]</sup>

In a recent pioneering study the  $pK_a$ s of ionizable ligands immobilized on nanoparticles (NPs) were determined through potentiometry, and compared with theoretical calculation studies.<sup>[33]</sup> It was shown that apparent  $pK_a$ s of NP-immobilized ligands were significantly higher than those of the free ligands in solution. The apparent  $pK_a$  increased with increasing both NPs and cation size, while decreased with increasing salt concentration (particularly for salt concentration  $< 0.05$  M). Even for very low concentrations of NPs, the local environment of the acid groups determines, through a balance of chemical free energy, electrostatic, van der Waals, steric, and packing interactions, its protonation state. The degree of dissociation was affected by the restriction/immobilization of the –COOH groups on the NPs surface and, possibly, by other factors such as NPs curvature.<sup>[33]</sup>

Figure 2 shows the speciation plot of SBA-TETA and SBA-15. At neutral pH SBA-TETA is positively charged ( $[(MMs)H_4]^{4+}$ ), while SBA-15 is not dissociated and remains uncharged.

The copper and zinc complexation by SBA-TETA and SBA-15 was then investigated through potentiometry (Figure 3). Copper complexation starts at very low pH, since at pH 2 about 50% of  $Cu^{2+}$  ions are already bound to SBA-TETA (Figure 3A). The  $\log K$  values of the formed complexes are lower than protonation constants of the free SBA-TETA (Table 2). This suggests the involvement of all dissociated groups in the metal coordination. Above pH 3, the protons of  $[Cu(SBA-TETA)H_4]^{5+}$  complex dissociates, and only at pH 9 all nitrogen atoms of TETA ligand are involved in metal chelation. Even at basic pH copper complexes with SBA-TETA remain stable.

The studies of metal complex formation with SBA-TETA were performed at 2:1, 1:1, and 1:2 metal:ligand molar ratios and the obtained results were analyzed with Hyperquad software. Only 1:1 metal:ligand stoichiometry was formed (Table 2) and further confirmed by EPR studies.

HySS program allowed to calculate  $pM$  parameter (on the base of  $\log \beta$  in Table 2). The higher the  $pM$ , the lower the concentration of free  $M^{n+}$  in solution. Hence a high  $pM$  means a high stability of metal–ligand complexes. The  $pM$  value depends on the pH of the aqueous solution. Figure 4 shows that the  $pM$  of both  $Cu^{2+}$  and  $Zn^{2+}$  in the presence of SBA-TETA sharply increases already at pH 4 meaning that copper and zinc can be strongly adsorbed on that functionalized mesoporous silica.

Table 2 reports  $pM$  at pH 7.4 for SBA-TETA complexes with copper in comparison with the respective complexes with free TETA ligand. The  $pCu$  (=16.1) value for SBA-TETA complexes is slightly lower than the corresponding  $pCu$  value of Cu-TETA complexes ( $pCu^{TETA} = 17.1$ ). The lowering of  $pCu$  can be caused by the rigidity of the TETA ligand bound to the mesoporous material, which may make difficult obtaining planar copper



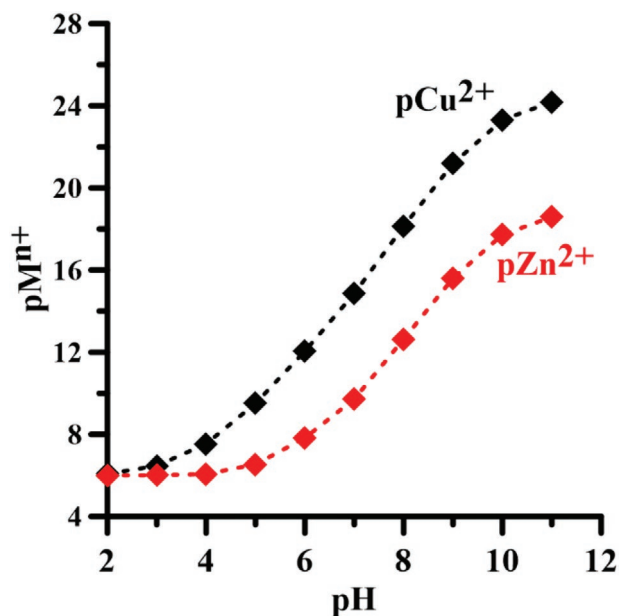


**Figure 4.** Relationship between  $pMn^{+}$  of SBA-TETA and growing pH values.

coordination, which is characteristic for free TETA chelate with copper ions.<sup>[34]</sup>

The stoichiometry of zinc complexes is the same of that of copper complexes (metal:ligand = 1:1), although the stability is slightly lower (Table 2). The  $[Zn(SBA-TETA)H_4]^{5+}$  complexes start to form above pH 2 and to carry out proton dissociation at pH 4, where only about 50% of zinc ions are bound. The log  $K$  values of zinc complexes are lower than respective protonation constants of free ligand and it is likely that all ligand binding sites are involved in the zinc coordination. At the reference pH 7.4, zinc complexes with SBA-TETA ( $pZn = 10.8$ ) are more stable than those with free TETA ( $pZn^{TETA} = 8.4$ ) and in equimolar ligand and metal solution 100% of zinc ions remain bound to SBA-TETA in the pH range 6–9 (Figure 3B). The coordination number and the geometry of zinc complexes depend only on ligand size and charge, while there are no ligand field stabilization effects and nor constraints on complex geometry as in the case of copper complexes.<sup>[35]</sup> In most zinc complexes a slightly distorted tetrahedral coordination frequently occurs.<sup>[35]</sup> This enhances Lewis acidity of the metal center as well as the acidity of a coordinated water molecule.

In contrast to SBA-TETA, SBA-15 does not form stable complexes neither with copper nor with zinc ions (Figure 2C,D). Only above pH 6, SBA-15 forms weak metal complexes with low stability constants (Table 2). This confirms the importance of TETA grafting on SBA-15 to obtain an effective adsorbent.

#### 4.1. Comparison between the Potentiometric Data and the Data Obtained from the Adsorption Isotherm

In recent studies, the isotherms of copper and zinc ions were studied by means of ICP-OES. The adsorption pH = 4 was chosen after the analysis of speciation diagrams of copper and

zinc hydrolysis (Figure S2, Supporting Information), while at this pH there is no precipitation of copper and zinc hydroxides. 15 mg of SBA-TETA were treated for 24 h at 25 °C with 10 mL solution containing growing concentration of metal ion. The obtained results showed that SBA-TETA adsorbs copper at a higher extent than zinc. Indeed, the maximal adsorbed amounts, are 23.9 and 13.6 mg g<sup>-1</sup> for copper and zinc, respectively.<sup>[21]</sup> The maximal loading of copper on SBA-TETA is comparable to 29.1 mg g<sup>-1</sup> the value obtained by mean of potentiometric titrations (see Figure 3A; pH 4). The slight discrepancy between the two values can be attributed to a higher experimental error of ICP-OES respect to potentiometric measurements. Indeed, the experimental method used before ICP measurements require an additional sample filtration step and do not permit a strict control of pH during metal adsorption process on SBA-TETA.

As far as zinc is concerned, potentiometric measurements (see Figure 3B; pH 4) show the maximum metal loading 18.5 mg g<sup>-1</sup>. In this case the greatest discrepancy, in addition to the same probable reasons set out above for copper, may be due to the fact that the zinc complex is less stable and perhaps after a treatment period of 24 h, part of complexes hydrolyzes.

##### 4.1.1. Competitive Adsorption of Cu<sup>2+</sup> and Zn<sup>2+</sup> on SBA-TETA

Theoretical speciation studies with HySS program<sup>[25]</sup> allow to evaluate the competition between two (or more) metal ions for ligand binding sites in solution. This approach was recently used to evaluate the competition between copper and zinc ions toward free TETA.<sup>[20]</sup> In this work, speciation studies, carried out by means of HySS software,<sup>[25]</sup> were used to evaluate the free metal ion content in the solution after treatment with SBA-TETA (Table 3). The HySS software uses the protonation constants (Table 1) and complexes formation constants (Table 2) of SBA-TETA with both copper and zinc ions but does not consider the formation of mixed SBA-TETA-Cu-Zn complexes. Cu<sup>2+</sup> ions bind more preferably to SBA-TETA than and Zn<sup>2+</sup> ions. The results were compared with ICP-AES experimental data in the same ligand and metals concentration conditions.

According to the theoretical competition studies with HySS program (see Section 2.4.1), SBA-TETA in the equimolar metal ion solution, can coordinate both metal ions (Figure 5A) and there are still free metal binding sites (free ligand: (SBA-TETA)H<sub>5</sub>, (SBA-TETA)H<sub>4</sub>, and (SBA-TETA)H<sub>3</sub>, Figure 5A). In the same theoretical calculations with a ten times excess of zinc ions (Figure 5B) all metal binding sites are saturated above pH 4, and the excess of zinc forms Zn(OH)<sub>2</sub> above pH 8. At pH 4 the calculated free copper and zinc concentrations are 0.08 and 64.97 ppm, respectively.

The theoretical calculations were compared with experimental data. In the solution containing 10 ppm metal concentration the remaining free copper content was 0.01 ppm (theoretical calculation 0.10 ppm), while zinc concentration was 1.20 (theoretical calculation 0.2 ppm). In the solution containing a Zn:Cu = 10:1 concentration ratio, 3.2 ppm of copper (theoretical calculation 0.08 ppm) and 81.7 ppm (theoretical concentration 64.97 ppm) of zinc ions remained unbound. The differences



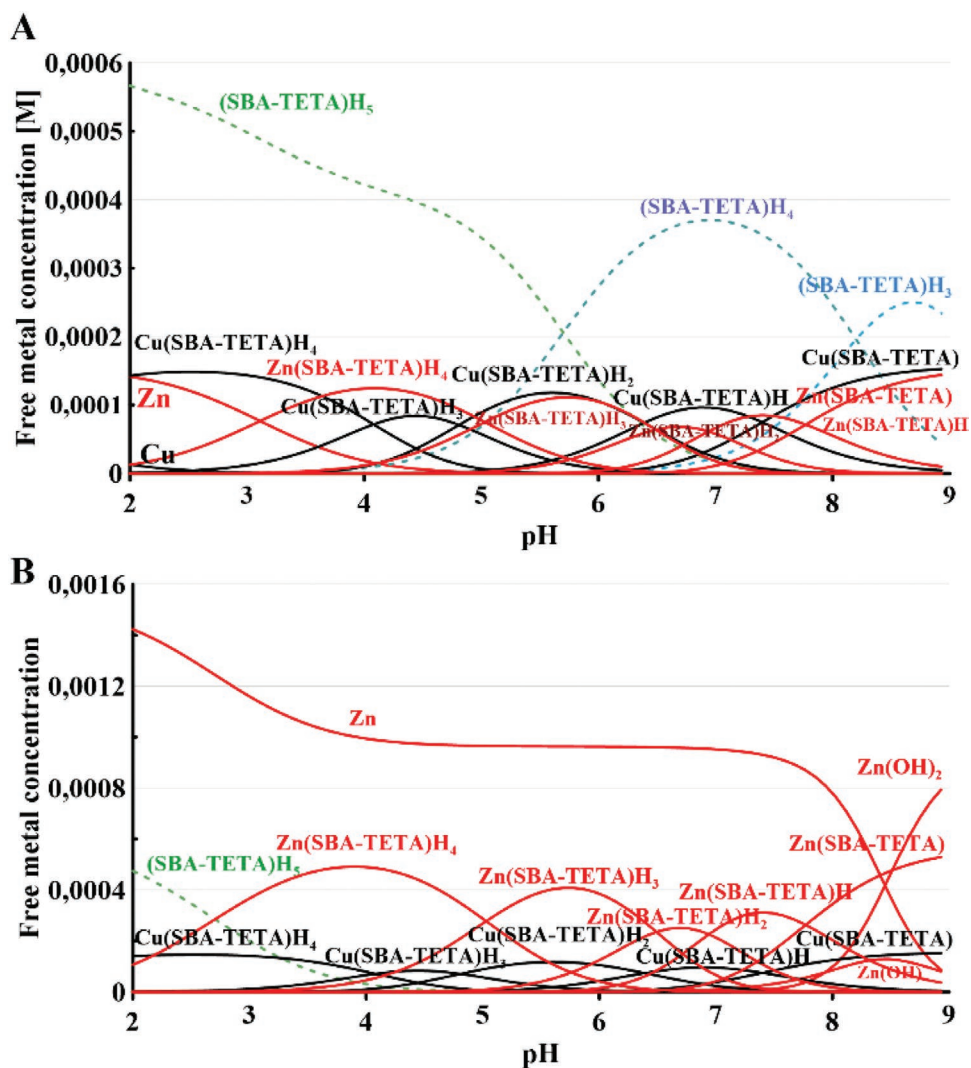


**Figure 5.** Theoretical competition studies between zinc and copper ions with SBA-TETA calculated with HySS program on the base of the protonation constants (Table 2) and complex formation constants ( $\log \beta$ ) of SBA-TETA in Table 3: A) MMs functionalized with  $[TETA] = 7.24 \times 10^{-4}$  M,  $[Cu^{2+}] = 1.57 \times 10^{-4}$  M (10 ppm), and  $[Zn^{2+}] = 1.53 \times 10^{-4}$  M (10 ppm); B) MMs functionalized with  $[TETA] = 7.24 \times 10^{-4}$  M,  $[Cu^{2+}] = 1.57 \times 10^{-4}$  M (10 ppm), and  $[Zn^{2+}] = 1.53 \times 10^{-3}$  M (100 ppm).

between theoretical and experimental data are likely due to the experimental errors of ICP-AES measurements (filtration of the samples, high LOQ) without pH control during experiment or due to the formation of mixed SBA-TETA-Cu-Zn complexes with different stability constants. Potentiometry is a highly precise technique and as shown in our studies, can be used for ligand grafting quantification as well as for the determination of surface charge. Next to the metal-complex stability constant data, potentiometry provides the maximum metal loading data. The greatest advantage of potentiometry is the lack of buffer solutions, which influence metal coordination studies by competition with ligand for metal binding sites or/and formation of mixed metal-ligand-buffer complexes.<sup>[36]</sup>

The complex formation stability constants provide important data of complex stability and can be used for theoretical competition studies in biological systems (e.g., in human serum competition with Human Serum Albumin), where experimental

data are difficult to obtain. The SC-Database provides access to published stability constants for metal complexes of  $\approx 9800$  ligands.<sup>[37]</sup> and deliver data for competition studies.

## 4.2. Spectroscopic Metal Complex Characterization

In order to investigate metal coordination sites (previously indicated in the potentiometric studies) and geometry of the zinc and copper complexes, three distinct spectroscopic techniques were used.

### 4.2.1. Zinc Complex Characterization by ssNMR

NMR spectroscopy is a potent analytical tool for identification of the chemical composition of a given sample.<sup>[38]</sup> In this

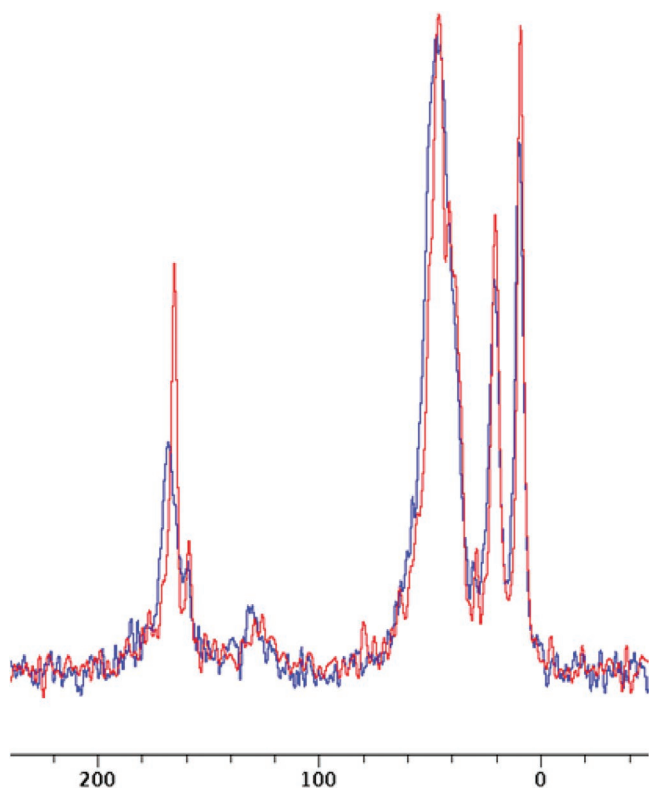


**Figure 6.**  $^{13}\text{C}$  solid state NMR spectra of SBA-TETA (red) before and after  $\text{Zn}^{2+}$  ion adsorption (blue).

study, we investigate the interaction between  $\text{Zn}^{2+}$  ions and SBA-TETA, using solid state 400 MHz NMR spectrometers. **Figure 6** shows the NMR spectra of before and after  $\text{Zn}^{2+}$  ion adsorption. The figure shows clear shift mainly in the peak

observed around 175 ppm proposing that the ion interaction is mainly through the nitrogen sites atoms.

#### 4.2.2. Copper Complex Characterization by EPR

EPR known also as electron spin resonance is a potent tool to probe species with unpaired electrons such as the organic free radicals<sup>[15,39]</sup> and the paramagnetic transition metals.<sup>[40–42]</sup> EPR is an analog of NMR as it provides chemical and structural information by probing the electron spin rather than the nuclear spin. The existence of unpaired electrons is common as electrons usually paired forming diamagnetic molecules, making EPR superior for selective sites studies. For example one can study the specific binding site of macromolecules such as the heme group in hemoglobin and myoglobin offering a powerful tool to monitor only the active sites in the macromolecules.<sup>[42,43]</sup> Moreover, EPR can be used to screen reactions that involve paramagnetic reactive intermediates, elucidate the structure of paramagnetic inorganic molecules, and to determine the oxidation state of transition metal ions.<sup>[41,44]</sup> For example, copper can have different oxidation states such as  $\text{Cu}^+$  and  $\text{Cu}^{2+}$  where  $\text{Cu}^+$  is  $d^{10}$  system with no unpaired electron hence no EPR signal can be observed while  $\text{Cu}^{2+}$  is  $d^9$  with one unpaired electron that can be detected by EPR spectroscopy. Moreover, EPR spectrum contains information about all interactions of the unpaired electron spin and the magnetic moments of nuclei spin in the vicinity of the electron spin.<sup>[41,45]</sup> Thus, EPR spectroscopy is widely used for structural elucidation of inorganic copper complexes and copper enzymes in addition to confirm copper binding with biomolecules. In this study we employed x-band EPR spectroscopy to investigate copper interaction with SBA-TETA. **Figure 7** shows the x-band EPR at 100 K of SBA-TETA after copper adsorption and the

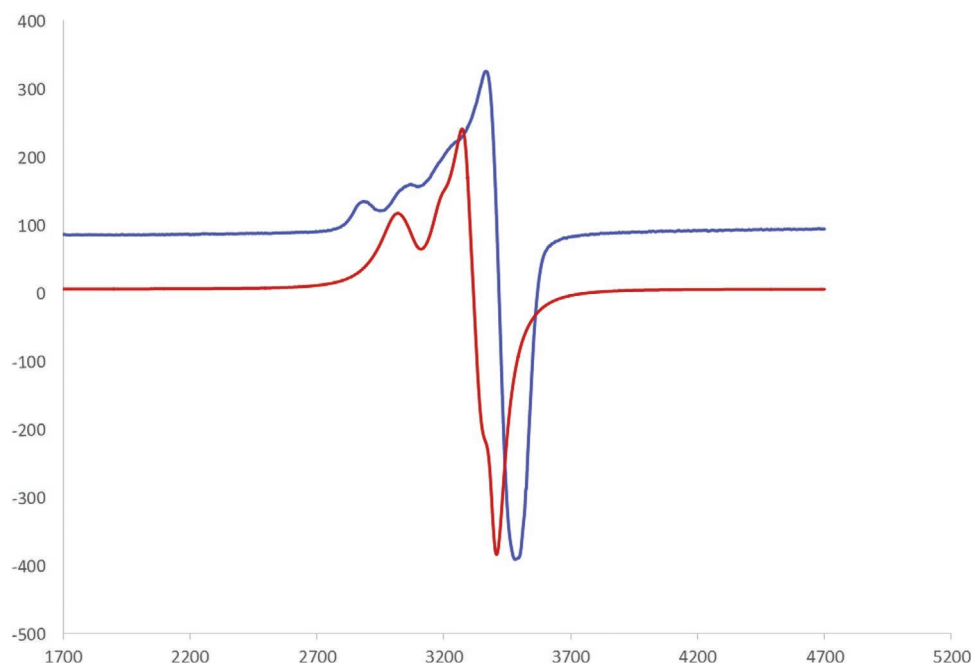


**Figure 7.** CW EPR spectra of copper-SBA-TETA (blue) and free copper salt (red) recorded at 100 K.

**Table 4.** EPR parameters of the free copper and copper complexes with SBA-TETA compared with the literature data.<sup>[46]</sup>

Assumed composition of the complex	Obtained EPR results			Assumed composition of the complex	Literature EPR results <sup>a)</sup>		
	$A_{  } \pm 3, G$	$g_{  } \pm 0.0005$	$g_{\perp} \pm 0.0005$		$A_{  } \pm 3, G$	$g_{  } \pm 0.005$	$g_{\perp} \pm 0.005$
Cu(NO <sub>3</sub> ) <sub>2</sub>	170	2.1778	2.1223	Cu(H <sub>2</sub> O) <sub>6</sub> <sup>2+</sup>	117	2.420	2.091
Cu-SBA-TETA	182	2.2306	2.0661	Cu(TETA)Cl <sub>2</sub>	184	2.200	2.072
Cu-SBA-(TETA) <sub>2</sub> Cl <sub>2</sub>	–	–	–	Cu(TETA) <sub>2</sub> Cl <sub>2</sub>	164	2.201	2.070

<sup>a)</sup>Solution of Cu(NO<sub>3</sub>)<sub>2</sub> in an ethanol–water mixture (1:1), solution of TETA and CuCl<sub>2</sub> (2:1) in ethanol, solution of TETA and CuCl<sub>2</sub> (4:1) in ethanol, respectively.

copper spectrum of used copper salt ions. The figure shows a clear difference between the free copper salts ions compared with the spectrum of copper-SBA-TETA providing an evidence of copper interaction with SBA-TETA. The results show significant differences of both  $g$ -values and hyperfine coupling constant ( $A_{||}$ ) of the copper salt and Cu-SBA-TETA complex (Table 4). The results confirmed that SBA-TETA completely coordinated copper with without any remaining free copper traces.

In order to determine the composition of copper complexes formed on the surface of SBA-TETA, we analyzed the EPR spectra of Cu and Cu/SBA-TETA system (Figure 7). This allowed us to obtain the spin Hamiltonian parameters  $g_{||}$ ,  $g_{\perp}$ , and  $A_{||}$  for the spectra of copper complexes and to compare them with reference spectra of free TETA with copper ions<sup>[46]</sup> (Table 4) found in literature.

The parameters of red line correspond to Cu(NO<sub>3</sub>)<sub>2</sub> complex of copper and are consistent with the literature data, while blue line data refer to Cu/SBA-TETA sample obtained with an excess of copper ions (See Section 2.6). The estimated values (Table 4) and a comparison with published data allowed us to suggest that the complex formed on the surface of SBA-TETA has the composition Cu(TETA)Cl<sub>2</sub>, while polyamine complexes are not formed. The copper complex has distorted square planar conformation, due to the presence of silanol in the metal coordination core.

#### 4.2.3. Copper Complex Characterization by UV–vis

The comparison of lyophilized samples with the same hydrated samples (and dried under vacuum, see Section 2.6) of SBA-15, SBA-NH<sub>2</sub>, and SBA-TETA (Figure S3, Supporting Information) shows clearly the presence of water molecule in the copper coordination shell of all studied samples.

The Cu/SBA-TETA sample has a blue color, Cu/SBA-NH<sub>2</sub> is green, while Cu/SBA-15 does not coordinate copper ions and has pale blue color of Cu(H<sub>2</sub>O)<sub>6</sub><sup>2+</sup> complex (Figure S4, Supporting Information). The UV–vis spectra of Cu/TETA and Cu/SBA-TETA (Figure S4, Supporting Information) show clearly d-d transitions and confirm direct inclusion of copper ions in the amine complex. The  $\lambda_{\max}$  at 440 nm for Cu/TETA system can be attributed to a distorted square planar conformation. In the Cu/SBA-TETA system, the  $\lambda_{\max}$  is shifted to the longer wavelengths due to the presence of Cu–O bond and participation of silanol in metal coordination core.

## 5. Conclusions

SBA-TETA is a mesoporous material functionalized with TETA copper and zinc chelating agent. SBA-TETA joins versatility of mesoporous materials to load a large amount of cargo, environmental-friendly, and bioavailability, with TETA high efficiency in metal coordination. Such a combination gives an efficient tool for medical diagnostic, theragnostic, or metal clearance, but before being used, SBA-TETA complexes and their water solution equilibria need to be described. Potentiometry technique was used for the first time for ligand content quantification in the SBA-TETA material and for the determination of metal complex formation constants. Moreover, metal complexes were characterized by EPR and ssNMR spectroscopy. The obtained data were compared with classical adsorption studies giving rewarding results. Potentiometry is a fast and economic technique, which can be used for water solution equilibria studies with metal ions and deliver stability data of the formed complexes, which are necessary to establish possible competition reactions with human endogenous molecules and metal ions. In summary, potentiometric studies deliver more precise data of metal coordination studies respect to more popular techniques for the characterization of mesoporous materials and permit theoretical competition studies with other ligands in solution.

## Supporting Information

Supporting Information is available from the Wiley Online Library or from the author.

## Acknowledgements

A.S. acknowledges financial support from FIR 2019 and MIUR (FFABR 2017).

## Conflict of Interest

The authors declare no conflict of interest.

## Keywords

electron paramagnetic resonance, metal coordination, nuclear magnetic resonance, potentiometry, speciation diagrams

Received: March 26, 2020

Revised: April 21, 2020

Published online:

- [1] a) M. Lovell, J. Robertson, W. Teesdale, J. Campbell, W. Markesbery, *J. Neurol. Sci.* **1998**, *158*, 47; b) A. I. Bush, *Trends Neurosci.* **2003**, *26*, 207.
- [2] P. A. Adlard, A. I. Bush, *J. Alzheimer's Dis.* **2006**, *10*, 145.
- [3] J. L. Vivero-Escoto, R. C. Huxford-Phillips, W. Lin, *Chem. Soc. Rev.* **2012**, *41*, 2673.
- [4] K. S. Siddiqi, A. Husen, S. S. Sohrab, M. O. Yassin, *Nano. Res. Lett.* **2018**, *13*, 231.
- [5] a) G. Liu, P. Men, P. L. Harris, R. K. Rolston, G. Perry, M. A. Smith, *Nano Lett.* **2006**, *406*, 189; b) G. Liu, P. Men, G. Perry, M. A. Smith, in *Progress in Brain Research*, Vol. 180, Elsevier, New York **2009**, p. 97.
- [6] D. McLachlan, T. P. Kruck, W. J. Lukiw, S. S. Krishnan, *Can. Med. Assoc. J.* **1991**, *145*, 793.
- [7] a) C. Loske, A. Gerdemann, W. Schepl, M. Wycislo, R. Schinzel, D. Palm, P. Riederer, G. Münch, *Eur. J. Biochem.* **2000**, *267*, 4171; b) C. W. Ritchie, A. I. Bush, A. Mackinnon, S. Macfarlane, M. Mastwyk, L. MacGregor, L. Kiers, R. Cherny, Q.-X. Li, A. Tammer, *Arch. Neurol.* **2003**, *60*, 1685.
- [8] G. Liu, P. Men, W. Kudo, G. Perry, M. A. Smith, *Nano Lett.* **2009**, *455*, 187.
- [9] I. W. Hamley, *Chem. Rev.* **2012**, *112*, 5147.
- [10] L. Miller, G. Winter, B. Baur, B. Witulla, C. Solbach, S. Reske, M. Lindén, *Nanoscale* **2014**, *6*, 4928.
- [11] J. E. Lee, N. Lee, T. Kim, J. Kim, T. Hyeon, *Acc. Chem. Res.* **2011**, *44*, 893.
- [12] L. Yi, T. Wu, W. Luo, W. Zhou, J. Wu, *Neural Regener. Res.* **2014**, *9*, 69.
- [13] a) Q. He, Z. Zhang, F. Gao, Y. Li, J. Shi, *Small* **2011**, *7*, 271; b) X. He, H. Nie, K. Wang, W. Tan, X. Wu, P. Zhang, *A Chemistry* **2008**, *80*, 9597.
- [14] S. Bhattacharyya, M. Dixit, *Dalton Trans.* **2011**, *40*, 6112.
- [15] S. Al-Harathi, J. I. Lachowicz, M. E. Nowakowski, M. Jaremko, Ł. Jaremko, *J. Inorg. Biochem.* **2019**, *198*, 110716.
- [16] D. C. Crans, *Coord. Chem. Rev.* **2017**, *352*, 398.
- [17] D. L. Suarez, S. Goldberg, C. Su, *Mineral-Water Interfacial Reactions*, Vol. 715, ACS Symposium Series, American Chemical Society, Washington, DC **1998**, pp. 136–178.
- [18] T. de F. Paulo, H. D. Abruña, I. C. N. Diógenes, *Langmuir* **2012**, *28*, 17825.
- [19] P. W. Schindler, in *Metal Ions in Biological Systems*, Vol. 18, Marcel Dekker Inc., New York/Basel **1984**, p. 105.
- [20] V. M. Nurchi, G. Crisponi, M. Crespo-Alonso, J. I. Lachowicz, Z. Szewczuk, G. J. Cooper, *Dalton Trans.* **2013**, *42*, 6161.
- [21] J. I. Lachowicz, G. R. Delpiano, D. Zanda, M. Piludu, E. Sanjust, M. Monduzzi, A. Salis, *J. Environ. Chem. Eng.* **2019**, *7*, 103205.
- [22] L. Medda, M. F. Casula, M. Monduzzi, A. Salis, *Langmuir* **2014**, *30*, 12996.
- [23] a) W. Wu, W. Guo, Z. Ji, Y. Liu, X. Hu, Z. Liu, *J. Dispersion Sci. Technol.* **2018**, *39*, 594; b) M. Barczak, *J. Solid State Chem.* **2018**, *258*, 232.
- [24] G. Gran, *Analyst* **1952**, *77*, 661.
- [25] L. Alderighi, P. Gans, A. Ienco, D. Peters, A. Sabatini, A. Vacca, *Coord. Chem. Rev.* **1999**, *184*, 311.
- [26] A. Albert, E. P. Serjeant, *Ionization Constants of Acids and Bases: A Laboratory Manual*, Methuen, London **1962**.
- [27] T. Kiss, É. A. Enyedy, T. Jakusch, *Coord. Chem. Rev.* **2017**, *352*, 401.
- [28] I. Nagypál, M. Beck, *Coord. Chem. Rev.* **1982**, *43*, 233.
- [29] A. E. Martell, R. J. Motekaitis, *Determination and Use of Stability Constants*, VCH publishers, Hoboken, NJ **1992**.
- [30] G. Berthon, *Handbook of Metal-Ligand Interactions in Biological Fluids*, Marcel Dekker, NY **1995**.
- [31] Z. Wu, D. Zhao, *Chem. Commun.* **2011**, *47*, 3332.
- [32] J. I. Lachowicz, V. M. Nurchi, G. Crisponi, M. de Guadalupe Jaraquemada-Pelaez, M. Ostrowska, J. Jezierska, E. Gumienna-Kontecka, M. Peana, M. A. Zoroddu, D. Choquesillo-Lazarte, *J. Inorg. Biochem.* **2015**, *151*, 94.
- [33] D. Wang, R. J. Nap, I. Lagzi, B. Kowalczyk, S. Han, B. A. Grzybowski, I. Szleifer, *J. Am. Chem. Soc.* **2011**, *133*, 2192.
- [34] P. Comba, S. P. Gavrish, Y. D. Lampeka, P. Lightfoot, A. Peters, *J. Chem. Soc., Dalton Trans.* **1999**, *1999*, 4099.
- [35] R. R. Crichton, *Biological Inorganic Chemistry: A New Introduction to Molecular Structure and Function*, Elsevier, NY **2012**.
- [36] M. T. Beck, I. Nagypál, *Chemistry of Complex Equilibria*, Vol. 30, Akadémiai Kiadó, Budapest **1990**, p. 141.
- [37] SCQuery, The IUPAC Stability Constants Database, Academic Software (Version 5.5), Royal Society of Chemistry, Cambridge **1993**, 2005.
- [38] a) P. Westermark, U. Engström, K. H. Johnson, G. T. Westermark, C. Betsholtz, *Proc. Natl. Acad. Sci. USA* **1990**, *87*, 5036; b) D. F. Moriarty, D. P. Raleigh, *Biochemistry* **1999**, *38*, 1811.
- [39] a) S. M. Mattar, A. H. Emwas, *Chem. Phys. Lett.* **2003**, *368*, 724; b) S. M. Mattar, A. H. Emwas, L. A. Calhoun, *J. Phys. Chem. A* **2004**, *108*, 11545; c) J. Al-Nu'airat, B. Z. Dlugogorski, I. Oluwoye, X. Gao, M. Altarawneh, *Proc. Combust. Inst.* **2019**, *37*, 3091; d) G. Fang, X. Chen, W. Wu, C. Liu, D. D. Dionysiou, T. Fan, Y. Wang, C. Zhu, D. Zhou, *Environ. Sci. Technol.* **2018**, *52*, 14352; e) S. M. Mattar, A. H. Emwas, A. D. Stephens, *Chem. Phys. Lett.* **2002**, *363*, 152.
- [40] a) S. M. Mattar, A. D. Stephens, A. H. Emwas, *Chem. Phys. Lett.* **2002**, *352*, 39; b) A. H. M. Emwas, Z. A. Al-Talla, X. Guo, S. Al-Ghamdi, H. T. Al-Masri, *Magn. Reson. Chem.* **2013**, *51*, 255; c) S. Ghosh, V. Garcia, K. Singewald, S. M. Damo, S. Saxena, *Appl. Magn. Reson.* **2018**, *49*, 1299; d) T. Matsuo, T. Kono, I. Shobu, M. Ishida, K. Gonda, S. Hirota, *Chem. - Eur. J.* **2018**, *24*, 2767.
- [41] H. Liang, C. Xia, A.-H. Emwas, D. H. Anjum, X. Miao, H. N. Alshareef, *Nano Energy* **2018**, *49*, 155.
- [42] X.-C. Su, J.-L. Chen, *Acc. Chem. Res.* **2019**, *52*, 1675.
- [43] a) F. Alahmari, B. Davaasuren, A.-H. Emwas, P. M. Costa, A. Rothenberger, *Inorg. Chim. Acta* **2019**, *488*, 145; b) L. M. Moreira, A. L. Poli, J. P. Lyon, F. Aimbire, J. C. Toledo Jr, A. J. Costa-Filho, H. Imasato, *J. Porphyrins Phthalocyanines* **2010**, *14*, 199.
- [44] D. A. Svistunenko, J. Dunne, M. Fryer, P. Nicholls, B. J. Reeder, M. T. Wilson, M. G. Bigotti, F. Cutruzzola, C. E. Cooper, *Biophys. J.* **2002**, *83*, 2845.
- [45] a) H. Ouellet, K. Rangelova, M. LaBarre, J. B. Wittenberg, B. A. Wittenberg, R. S. Magliozzo, M. Guertin, *J. Biol. Chem.* **2007**, *282*, 7491; b) A. Tyryshkin, S. Dikanov, E. Reijerse, C. Burgard, J. Hüttermann, *J. Am. Chem. Soc.* **1999**, *121*, 3396; c) E. G. Evans, M. J. Pushie, K. A. Markham, H.-W. Lee, G. L. Millhauser, *Structure* **2016**, *24*, 1057.
- [46] Y. Shenberger, A. Shimshi, S. Ruthstein, *J. Phys. Chem. B* **2015**, *119*, 4824.